



**HAL**  
open science

## **Polar stratospheric clouds climatology over Dumont d'Urville between 1989 and 1993 and the influence of volcanic aerosols on their formation**

Christine David, Slimane Bekki, Sophie Godin, Gérard Mégie, M. P. Chipperfield

### ► To cite this version:

Christine David, Slimane Bekki, Sophie Godin, Gérard Mégie, M. P. Chipperfield. Polar stratospheric clouds climatology over Dumont d'Urville between 1989 and 1993 and the influence of volcanic aerosols on their formation. *Journal of Geophysical Research: Atmospheres*, 1998, 103 (D17), pp.22163-22180. 10.1029/98JD01692 . insu-03090207

**HAL Id: insu-03090207**

**<https://insu.hal.science/insu-03090207>**

Submitted on 29 Dec 2020

**HAL** is a multi-disciplinary open access archive for the deposit and dissemination of scientific research documents, whether they are published or not. The documents may come from teaching and research institutions in France or abroad, or from public or private research centers.

L'archive ouverte pluridisciplinaire **HAL**, est destinée au dépôt et à la diffusion de documents scientifiques de niveau recherche, publiés ou non, émanant des établissements d'enseignement et de recherche français ou étrangers, des laboratoires publics ou privés.

# Polar stratospheric clouds climatology over Dumont d'Urville between 1989 and 1993 and the influence of volcanic aerosols on their formation

C. David, S. Bekki, S. Godin, and G. Mégie

Service d'Aéronomie du CNRS, Institut Pierre-Simon Laplace, Université Paris VI, Paris, France

M. P. Chipperfield

Department of Chemistry, University of Cambridge, Cambridge, England

**Abstract.** The first polar stratospheric clouds (PSCs) climatology ever established from lidar data and relative to a specific site is presented here. It is based on lidar backscatter and depolarization measurements of PSCs carried out between 1989 and 1993 at Dumont d'Urville (66°S, 140°E), which is a primary station of the Network for Detection of Stratospheric Changes (NDSC). The climatology was subdivided based on the stratospheric sulphuric acid aerosol content (background aerosols in 1989–1991 and volcanic aerosols in 1992–1993 following the Mount Pinatubo eruption). PSCs were mainly observed in July and August. Very few water ice clouds (type II) were detected. Most of the PSCs tended to form around the peak in sulphuric acid aerosol, between 17 and 23 km in 1989–1991 and between 11 and 20 km in 1992–1993. This tendency suggests that sulphuric acid aerosols are very likely to act as condensation nuclei for PSCs. As shown by previous lidar studies [Browell *et al.*, 1990], two type I subclasses were identified: depolarizing (nonspherical) particles (type Ia) and nondepolarizing (spherical) particles (type Ib). No type Ia PSCs were detected above the nitric acid trihydrate (NAT) saturation temperature,  $T_{\text{NAT}}$ , lending support to the theory that NAT is the main component of type Ia PSCs. There was also no evidence of the existence of sulphuric acid tetrahydrate (SAT) in the data. Some type Ib PSCs were observed close to the frost point, showing that supersaturation with respect to NAT is a necessary, but not sufficient, condition for the existence of solid PSCs. No type Ib PSCs were clearly detected above  $T_{\text{NAT}}$  in 1989–1991 whereas 18% of the PSCs seem to be found at temperatures above  $T_{\text{NAT}}$  in 1992–1993. This difference might be linked to the  $\text{HNO}_3$  uptake by volcanic sulphuric acid particles starting at higher temperatures. The fraction of type Ia out of the total PSCs observations was lower in 1992–1993 than in 1989–1991. This difference was not found to be highly statistically significant.

## 1. Introduction

Polar stratospheric clouds (PSCs) condition the polar stratosphere for subsequent ozone loss over Antarctica by providing sites for heterogeneous reactions which convert chlorine reservoir species ( $\text{ClONO}_2$ ,  $\text{HCl}$ ) into active forms ( $\text{Cl}$ ,  $\text{ClO}$ ) [World Meteorological Organization, 1995]. Furthermore, they remove nitrogen compounds from the lower stratosphere via nitric acid ( $\text{HNO}_3$ ) uptake followed by gravitational sedimentation.

After being first observed from the ground [Stanford, 1973], large-scale PSCs were detected in both polar re-

gions in 1979 with the satellite instrument Stratospheric Aerosol Measurements II (SAM II) [McCormick *et al.*, 1982]. The first data on PSC physical characteristics were obtained during the Airborne Antarctic Ozone Expedition (AAOE) (*Journal of Geophysical Research*, 94, (D9) and 94 (D14), 1989) in 1987. Balloon-borne measurements of PSCs have been conducted at from McMurdo Station (78°S, 167°E) since 1987 [Hofmann and Deshler, 1991; Adriani *et al.*, 1992], and several years of observations are available from the Admunsen-Scott South Pole Station (90°S) [Rosen *et al.*, 1991, 1993]. In addition, lidar measurements at Syowa (65°S, 40°E) since 1983 [Iwasaka *et al.*, 1986], at Admunsen-Scott since 1987 [Fiocco *et al.*, 1992] and at McMurdo since 1991 [Gobbi *et al.*, 1991] have confirmed the intermittent presence of PSCs over the whole continent during the winter.

Copyright 1998 by the American Geophysical Union.

Paper number 98JD01692.  
0148-0227/98/98JD-01692\$09.00

These observations have shown that PSCs mainly form in the 12–25 km range and that their occurrence is tightly correlated to temperature minima [McCormick *et al.*, 1982]. The thermodynamically most stable  $\text{HNO}_3$  hydrate, nitric acid trihydrate (NAT), was the first realistic suggestion as the most likely component of PSC particles [Crutzen and Arnold, 1986; Toon *et al.*, 1986]. On the basis of their optical properties, PSCs were classified into two general types, I and II [Hamill *et al.*, 1988; Poole and McCormick, 1988]. Type I clouds that are observed at 5 to 7 K above the ice frost point, are believed to be mainly composed of  $\text{HNO}_3$ , and to have typical radii of about 1  $\mu\text{m}$ . Type II PSCs are thought to be water ice particles, with radii  $\geq 2 \mu\text{m}$ , forming at the frost point temperature. Analyses of Arctic lidar data revealed two subclasses of type I PSC, Ia and Ib [Browell *et al.*, 1990], both appearing at, or below, the NAT equilibrium threshold temperature. Type Ia particles exhibit low backscatter ratios and high depolarization ratios, and are consistent with nonspherical larger particles [Toon *et al.*, 1990]. Type Ib particles exhibit high backscatter ratios and low depolarization ratios, consistent either with numerous liquid particles or with nonspherical particles with sizes much smaller than the lidar wavelength.

The exact mechanisms for PSC formation are still a topic of great debate. First, as the temperature decreases, stratospheric sulphuric acid aerosols absorb water to maintain their composition in equilibrium with the ambient water vapor pressure [Steele and Hamill, 1981]. Then, after further cooling, PSCs form. Several modes of formation have been proposed. Poole and McCormick [1988] suggested that  $\text{H}_2\text{SO}_4/\text{H}_2\text{O}$  aerosols could freeze as sulphuric acid tetrahydrate (SAT) at sufficiently low temperatures and act as solid condensation nuclei for NAT particles at temperatures below the NAT saturation point ( $\approx 195 \text{ K}$  at 20 km, for 5 ppmv of  $\text{H}_2\text{O}$  and 10 ppbv of  $\text{HNO}_3$ ). In this view, the different classes of type I PSCs form according to the cooling rate experienced by the air masses (cooling rate  $\leq 5 \text{ K/d}$  for type Ia and  $> 5 \text{ K/d}$  for type Ib) [Toon *et al.*, 1990]. More recently, Molina *et al.* [1993] proposed that  $\text{H}_2\text{SO}_4/\text{H}_2\text{O}$  aerosols might remain supercooled even below the NAT equilibrium temperature. Type Ib could then be droplets of liquid ternary  $\text{H}_2\text{SO}_4/\text{HNO}_3/\text{H}_2\text{O}$  solution which form through rapid uptake of  $\text{HNO}_3$  by sulphuric acid aerosols at temperatures below the NAT saturation temperature, as observed at low sulphuric acid aerosols content (nonvolcanic situation) by Dye *et al.* [1992]. Temperatures for type Ib formation have never been observed for high  $\text{H}_2\text{SO}_4$  aerosol loadings. Observations of liquid  $\text{HNO}_3/\text{H}_2\text{O}$  films prior to NAT formation have been reported in the laboratory [Hanson, 1990]. Overall, the formation mechanism of solid particles above the frost point (type Ia PSCs) is still unclear, and several hypotheses for the freezing process have been suggested, including NAT freezing out of ternary solution [Molina

*et al.*, 1993; Tabazadeh *et al.*, 1994], NAT freezing out of binary  $\text{HNO}_3/\text{H}_2\text{O}$  solution during rapid temperature fluctuations [Meilinger *et al.*, 1995], and even heterogeneous nucleation of NAT on seed particles different from  $\text{H}_2\text{SO}_4/\text{H}_2\text{O}$  particles [Carslaw *et al.*, 1994; Iraci *et al.*, 1995]. A metastable phase, nitric acid dihydrate (NAD), might form first and then convert into NAT at lower temperatures [Worsnop *et al.*, 1993; Fox *et al.*, 1995]. Tabazadeh *et al.* [1995] suggested that amorphous solid solutions of  $\text{HNO}_3$  and  $\text{H}_2\text{O}$ , so-called type Ic PSC, could form during the warming of stratospheric aerosols which were in a glassy state. However, on the basis of laboratory data, Koop *et al.* [1995] argue that  $\text{H}_2\text{SO}_4$  or  $\text{HNO}_3$  hydrates could only form from water ice below the frost point but would then continue to exist up to their melting points. Whatever the formation mechanism, once formed, the solid particles would grow absorbing  $\text{HNO}_3$  and  $\text{H}_2\text{O}$  through condensational processes.

In this paper, we present a five year PSC climatology over Dumont d'Urville (66°S, 140°E), Antarctica, derived from lidar observations. The Mount Pinatubo (15°N, 120°E) eruption in June 1991 provided the opportunity of investigating the influence of volcanic particles on PSCs. Two periods are thus compared: 1989–1991, before the eruption when only background aerosols were present, and 1992–1993 after the global dispersion of Pinatubo aerosols was completed.

In section 2, the experimental setup is described together with the methodology used to retrieve the optical properties of the different scattering layers. Section 3 displays the observations and the method used to identify PSCs in the lidar signals is presented in section 4. Results and comparison of the two periods are shown in section 5. Interpretations of the observations, using a thermodynamic model, are discussed in section 6. Finally, the section 7 provides a summary of the results obtained.

## 2. Experimental Description and Methodology

The Polar Ozone Lidar Experiment (POLE) is a French Italian cooperation between the Service d'Aéronomie du CNRS and the IROE-CNR. POLE is a program of continuous monitoring of the stratosphere in the Antarctic, located at the French station Dumont d'Urville, which is a primary station of the Network for Detection of Stratospheric Changes (NDSC). At the present time, the lidar in Dumont d'Urville is the only one operating throughout the year on the Antarctic continent.

The backscatter lidar for aerosols and PSC measurements was set up in December 1988 and started operating in April 1989 [Sacco *et al.*, 1989]. During this first phase of the POLE experiment, the lidar included a frequency doubled Nd:YAG laser which emits 270 mJ with a 10-Hz repetition rate at the operating wavelength

of 532 nm [Stefanutti *et al.*, 1991]. The backscatter signal was collected on a 50-cm-diameter Newtonian telescope and split into two components polarized respectively parallel and perpendicular to the laser emission. Both components were detected by photomultiplier tubes with 10.5% quantum efficiency at 532 nm. The photomultipliers were gain switched to prevent saturation by the stronger returns from the lower altitudes. The signals were then time resolved using a 12-bit transient waveform recorder capable of storing 1024 samples with a resolution of 75 m. These digital samples were averaged on several shots before being recorded.

During the second phase of POLE, the first lidar system was improved and a DIAL lidar was set up in January 1991 to measure sequentially the vertical distributions of stratospheric ozone and of stratospheric aerosols and PSCs [Stefanutti *et al.*, 1992]. The 532 nm wavelength is still used for particle observations. The methodology for aerosols and PSC retrievals remained unchanged. The output energy of the pulsed Nd:YAG laser at 532 nm is now 450 mJ at 10-Hz repetition rate. The signal is received on a 80-cm-diameter Cassegrain telescope with aluminium coated optics. The two components polarized parallel and perpendicular to the laser emission are still recorded. The different wavelengths are separated using a grating spectrometer and further detected by photomultiplier tubes. Then the lidar signals are time resolved with a 30-m resolution and averaged before final data acquisition.

As the aerosols and PSC retrievals were essentially identical during the two phases, the data obtained before and after 1991 are consistent. Figure 1 shows an example of digitized raw signal profiles recorded on the June 24, 1993. Figure 1, which only represents a sample of the database profiles, illustrates well the good quality of the raw signal obtained by the instrument. The scale used here is meant to show the entire dy-

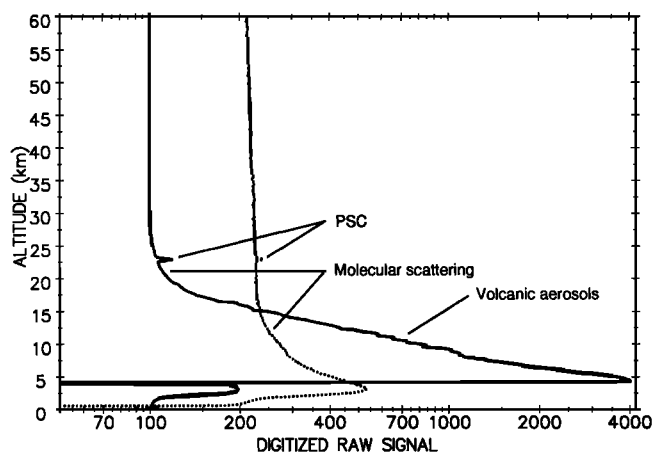


**Figure 1.** Example of lidar raw signals in the channels polarized parallel (solid line) and perpendicular (dotted line) to the laser emission on June 24, 1993 (the horizontal axis is logarithmic).

namic of the signal (note that the horizontal axis is logarithmic). The solid line gives the received signal in the polarization channel parallel to the laser emission, while the dashed line corresponds to the received signal in the perpendicular polarization. The receiver gain switching occurs between 3 and 8 km for the parallel channel and between 1 and 3 km for the perpendicular channel. On the parallel channel, the Mie scattering signals are seen from about 10 to 15 km due to volcanic aerosols and at about 23 km due to PSCs, superimposed to background aerosols. The Rayleigh scattering from the molecular atmosphere further decays with atmospheric density between 28 and 35-40 km. Above these altitudes, only a background signal is detected.

To reduce the statistical noise on an individual profile, the signals are averaged over 1000 shots (5 min) during polar night and 2000 shots (10 min) during daytime. A daily profile is defined as the average of all the individual profiles of that day. From the digitized raw signals, background levels are estimated using a linear or parabolic fit at higher altitudes (typically above 40 km) where backscattering by both molecules and particles is negligible. Then the range and background corrected signal is inverted using an algorithm based on the Klett [1981, 1985] method. The quantities derived from the combined Mie and Rayleigh components of the lidar signal include backscatter ratio and depolarization ratio, as defined in the next section.

## 2.1. Backscatter Ratio

The volume extinction coefficient  $\alpha(z)$  and backscatter coefficient,  $\beta(z)$  represent the sum of the contributions of both the Mie scattering by particles,  $\alpha_p(z)$  and  $\beta_p(z)$ , and the Rayleigh scattering by molecules,  $\alpha_m(z)$  and  $\beta_m(z)$ :

$$\beta(z) = \beta_m(z) + \beta_p(z) \quad (1)$$

$$\alpha(z) = \alpha_m(z) + \alpha_p(z) \quad (2)$$

Scattering by particles is usually characterized by the backscatter ratio  $R(z)$ , defined as

$$R(z) = 1 + \frac{\beta_p(z)}{\beta_m(z)} \quad (3)$$

To calculate the Rayleigh molecular backscatter coefficient, the absolute atmospheric density profiles are derived from local daily meteorological radiosondes. The extrapolation above the upper altitude of the radiosonde ( $\sim 20$  to 25 km in average) is made using a monthly zonal atmospheric model Middle Atmosphere Program, 1985 (MAP) at 65°S. The resulting uncertainty will be detailed in section 3.

Meanwhile, the determination of  $\beta(z)$  from the lidar equation requires quantitative knowledge of a relationship between  $\alpha(z)$  and  $\beta(z)$  [Klett, 1981]. If the value of the backscatter phase function is assumed to be known, these relationships are

$$\varphi_p(z) = \frac{\beta_p(z)}{\alpha_p(z)} \quad (4)$$

$$\varphi_m = \frac{\beta_m(z)}{\alpha_m(z)} \quad (5)$$

where  $\varphi_m$  is the Rayleigh backscatter phase function normalised for molecular scattering ( $\varphi_m \approx \frac{3}{8\pi} \approx 0.12 \text{ sr}^{-1}$ ) and  $\varphi_p(z)$  is the particles phase function. The estimation of  $\varphi_p(z)$  without the knowledge of the size, shape and refractive index of the aerosols is very difficult. In the classical Klett inversion procedure for single wavelength lidar measurements,  $\varphi_p$  is considered as constant with altitude and its value is then representative of the altitude where  $\beta_p(z)$  is maximal. In our methodology, before retrieving the optical properties of scattering layers, we first retrieve their geometrical characteristics, using a threshold method based on the variance of the range and background corrected signal [Chazette *et al.*, 1995]. Using this procedure, the bottom and top altitudes of a given scattering layer, distinct from molecular atmosphere, are determined. Particle phase function values were estimated for each layer from previous measurements or from Mie scattering models, according to the type of aerosols. Background stratospheric aerosols phase function is chosen at  $0.018 \text{ sr}^{-1}$  from an optical model [Rosen and Hofmann, 1986]. Volcanic aerosols phase function is estimated to be  $0.025 \text{ sr}^{-1}$  from lidar measurements at the Observatoire de Haute-Provence ( $44^\circ\text{N}$ ,  $5^\circ\text{E}$ ) [Chazette *et al.*, 1995]. As type II PSC scattering properties are close to those of cirrus clouds, their phase function is taken from the cirrus phase function, e.g.,  $0.055 \text{ sr}^{-1}$ . This value is also considered as an approximation for type I PSC phase function. This phase function profile provides the basic hypothesis for the Klett inversion method.

The determination of the total backscattering coefficient through the Klett procedure also requires a boundary condition: the knowledge of  $\beta_p(z)$  at a reference altitude  $z_r$ . To ensure the stability of the solution, this altitude is chosen above the aerosol layers, where the particle content is negligible and where scattering is only due to the molecular atmosphere, typically between 28 and 32 km, assuming therefore that the backscatter ratio  $R(z)$  is equal to unity at and above this reference altitude.

## 2.2. Depolarization Ratio

Detection of the signal on the polarization perpendicular to the laser emission allows the measurement of the depolarization ratio defined as

$$\delta(z) = \frac{\beta_{\perp}(z)}{\beta_{\parallel}(z)} \quad (6)$$

where  $\beta_{\perp}(z)$  and  $\beta_{\parallel}(z)$  are respectively the total backscatter coefficients in the parallel and perpendicular planes relative to the emitted polarization plane.

Calculated this way,  $\delta(z)$  includes depolarization from the molecular atmosphere, which is estimated to be about 1.5% [McNeil and Carswell, 1975; Kent *et al.*, 1990]. When the optical depth is sufficiently low (less than  $\sim 10^{-1}$  for most PSCs) contamination of the lidar return by multiple scattering is negligible [Platt, 1981].

The aerosol depolarization ratio (ratio of the intensity backscattered only by particles in the perpendicular channel to that backscattered only by particles in the parallel channel) is not used here because we found that it induces large mathematical instabilities in the altitude regions of low particle content. This parameter is only relevant for PSCs or for volcanic aerosols.

## 2.3. Uncertainties

Uncertainties in the determination of the total backscatter coefficient  $\beta(z)$  and therefore in the backscatter ratio  $R(z)$  were derived from the statistical analysis based on several years of data. They can be related to three main causes [Chazette *et al.*, 1995]:

1. The statistical fluctuations of the measured lidar signal associated with random detection processes; this uncertainty contributes to statistical errors of less than 2% to the backscatter ratio values on the parallel channel (parallel polarization to the laser emission) and between 5 to 10% on the perpendicular channel (perpendicular polarization to the laser emission), depending on the scattering matter (the uncertainty is lower for depolarizing matter, as the backscattered signal level is higher),

2. The presence of particles at and above the chosen reference altitude  $z_r$  and the subsequent uncertainty on the value of  $R(z_r)$ ; it is estimated to be less than 5% on the parallel channel and less than about 8 to 10% on the perpendicular channel,

3. The value of the particle phase function  $\varphi_p(z)$  and its altitude dependence; this uncertainty is estimated to be  $\approx 20\%$ .

The total uncertainty which results from these three causes on the parallel channel is less than 7% with the signal being significant up to 40 km [Chazette *et al.*, 1995]. On the perpendicular channel, the signal becomes very noisy above 25-30 km, resulting in a large uncertainty on the a priori knowledge of the backscattering coefficient at the reference altitude  $\beta(z_r)$ . Ac-

**Table 1.** Uncertainty on  $\delta(z)$  for Various Uncertainties on the Backscatter Ratio on the Perpendicular Channel, for a Fixed Uncertainty on the Backscatter Ratio of  $\approx 7\%$  on the Parallel Channel

Uncertainty on $R_{\perp}(z)$	Uncertainty on $\delta(z)$
10%	15 to 20%
15%	20 to 25%
20%	25 to 30%
25%	30 to 35%

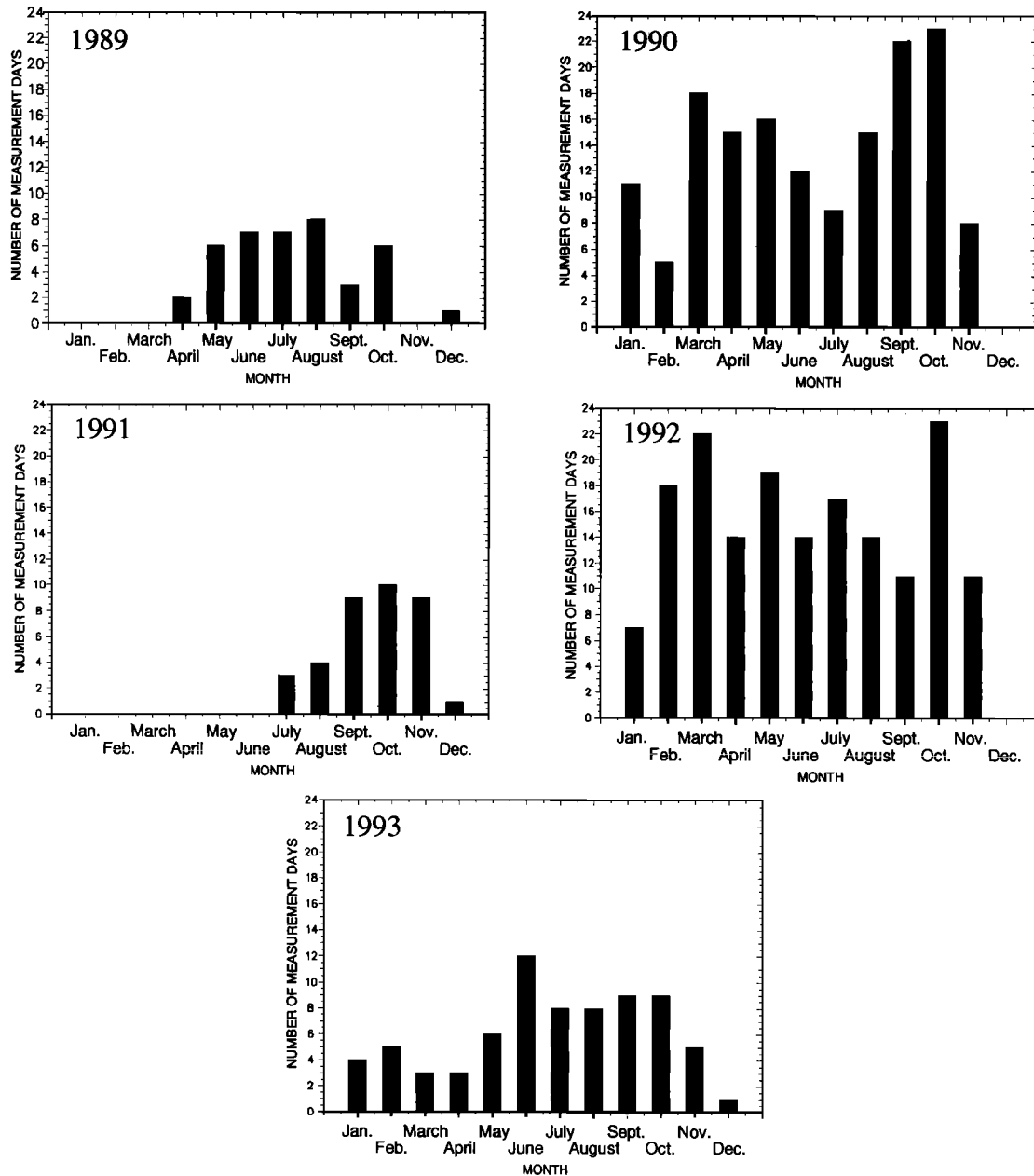


**Figure 2.** Number of days of valid lidar measurements per month at Dumont d'Urville between 1989 and 1993.

Accordingly, the total uncertainty on the perpendicular backscatter ratio (10 to 25%) is higher than on the parallel channel. The uncertainty on the depolarization ratio  $\delta(z)$  is primarily controlled by the uncertainty on the backscattering coefficient on the perpendicular channel. Table 1 gives the uncertainty on  $\delta(z)$  for various uncertainties on the backscatter ratio on the perpendicular channel, assuming a maximum uncertainty of 7% on the backscatter ratio on the parallel channel.

The contribution of each of the three errors mentioned above has an altitude dependence (according to the propagation of the errors at each step of the inversion [Chazette *et al.*, 1995]). Thus, to account on this uncertainty on the backscatter ratio and depolar-

ization ratio, only measurements with uncertainty on  $R_{\parallel}(z)$  lower than 10% and/or uncertainty on  $R_{\perp}(z)$  lower than 25% are taken into account and validated. The data set is thus reliable and consistent in terms of signal-to-noise ratio.

### 3. Observations

The lidar data presented in this paper were obtained between April 1989 and December 1993. Figure 2 presents the number of days of validated measurements per month. The low number of measurements in 1989 and 1991 originates from the difficulties encountered in implementing a lidar system in the extreme conditions

of the Antarctic. Two measurements per week were planned outside the period of PSC formation. This frequency had to be increased during winter and spring to produce a suitable dataset on PSCs. From June to September, when meteorological conditions are good (i.e., tropospheric cloud free atmosphere), observations are performed daily.

Three types of additional information are necessary to interpret the lidar data: the position of Dumont d'Urville with respect to the polar vortex, the temperature profile at the altitude range of the observed PSCs and the reference NAT and ice threshold temperatures. The position of Dumont d'Urville with respect to the polar vortex is evaluated on the 475K isentropic level ( $\approx 50$  hPa or 18 km). During wintertime, the polar vortex structure is such that if Dumont d'Urville is inside the vortex at 475K, it is very likely to be also inside the vortex at any levels of interest for PSC observations (i.e., between  $\approx 15$  km and  $\approx 28$  km) [Schoeberl *et al.*, 1992; Tuck *et al.*, 1989, 1992]. Ertel's potential vorticity maps at 475K are provided by the European Centre for Medium range Weather Forecasts (ECMWF). We consider here that values of potential vorticity greater than  $-35 \times 10^{-6} \text{ km}^2 \text{ kg}^{-1} \text{ s}^{-1}$  are outside the vortex, whereas values between  $-35$  and  $-55 \times 10^{-6} \text{ km}^2 \text{ kg}^{-1} \text{ s}^{-1}$  characterize the edge region, and values less than  $-55 \times 10^{-6} \text{ km}^2 \text{ kg}^{-1} \text{ s}^{-1}$  are inside the vortex [Schoeberl *et al.*, 1992; Tuck *et al.*, 1989, 1992].

Daily meteorological radiosondes provide temperature profiles. The mean altitude reached by the radiosondes is about 20–25 km. Some of them reach 30 km, while others do not exceed the tropopause height by more than a few kilometers. In this case, they are extrapolated using the monthly Middle Atmosphere Program, 1985 (MAP) climatology for  $65^\circ\text{S}$  in order to calculate molecular optical properties. As the MAP data are only mean zonal temperatures that tend to smooth out very low temperatures observed at the edge of the vortex, only radiosonde data are used in the interpretation of the PSC data. Consequently,  $\approx 30\%$  of the detected PSC (from 1989 to 1993) cannot be analysed in terms of temperature. Allowing for the uncertainty on radiosonde data, about 1 K for temperatures between 190 and 200 K [Parsons *et al.*, 1984], and the daily temperature variability between 1989 and 1993, the average uncertainty on the temperature is estimated to be 1–1.5 K between 16 and 20 km.

PSC formation is strongly controlled by saturation threshold temperatures which, in turn, depend on the cloud composition. As the two types of PSCs were first believed to be composed of NAT and ice, the radiosonde temperatures are compared to NAT and ice saturation temperatures ( $T_{\text{NAT}}$  and  $T_{\text{ice}}$ ). They are calculated using the Goff-Gratch formula [Murray, 1967] for the saturation water vapor pressure over ice and the Hanson and Mauersberger [1988] expression for  $\text{HNO}_3$  saturation vapor pressure over NAT. The mean  $\text{HNO}_3$  and  $\text{H}_2\text{O}$  profiles for this calculation are taken from

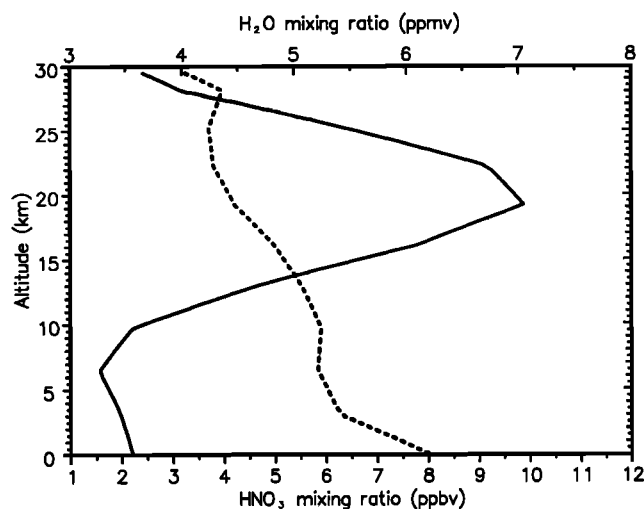


**Figure 3.**  $\text{HNO}_3$  (solid line) and  $\text{H}_2\text{O}$  (dotted line) mixing ratio profiles from LIMS data in average for April, at  $66^\circ 32'\text{S}$  [Gille *et al.*, 1984].

the Limb Infrared Monitor of the Stratosphere (LIMS) data (Figure 3) [Gille *et al.*, 1984]; they correspond to  $66^\circ 32'\text{S}$  averaged for April, just before the formation of the southern polar vortex. The  $\text{HNO}_3$  mixing ratio reaches 10 ppbv at 19 km, whereas the  $\text{H}_2\text{O}$  mixing ratio lies between 4 and 5.2 ppmv in the 10–30 km altitude range. These profiles are consistent with the more recent data from Upper Atmospheric Research Satellite (UARS) [Roche *et al.*, 1994]. It is worth pointing out that the profiles are not supposed to reproduce accurately the actual  $\text{HNO}_3$  levels during a particular winter, but rather to be representative of the average conditions prevailing over Dumont d'Urville. The calculation of  $T_{\text{NAT}}$  is only weakly sensitive to the uncertainty on the  $\text{HNO}_3$  mixing ratio. Indeed, at 50 hPa, for typical conditions, the  $\text{HNO}_3$  mixing ratio has to be multiplied by a factor 2 to increase  $T_{\text{NAT}}$  by about 1 K.

#### 4. Identification of PSCs on Lidar Signals

POLE data provide stratospheric vertical profiles of backscatter ratio and depolarization ratio. A backscatter ratio greater than unity is the signature of a scattering layer distinct from the molecular atmosphere. The depolarization ratio is an indicator of the nonsphericity of the particles and hence of their physical state. Combining these two parameters allows us to distinguish between stratospheric aerosols and PSCs and between the different types of PSCs. On the basis of previous lidar measurements [Kent *et al.*, 1986; Iwasaka *et al.*, 1986; Poole and McCormick, 1988; Toon *et al.*, 1989], the expected range of values of backscatter ratio and depolarization ratio at 532 nm for different types of aerosols and PSCs are summarized in Table 2. It should be noticed that according to this generic classification, PSCs,

**Table 2.** Stratospheric Aerosols and PSC Physical Characteristics and Lidar Optical Properties Converted at 532 nm From Previous Measurements.

Data are from *Kent et al.* [1986], *Iwasaka et al.* [1986], *Poole and McCormick* [1988], and *Toon et al.* [1989].

	Aerosols		PSC		
	background	volcanic	Type Ia	Type Ib	Type II
Shape	spherical	spherical	nonspherical	spherical	nonspherical
Mean radius	$\approx 0.07 \mu\text{m}$	$\approx 0.7 \mu\text{m}$	$\approx 1.0 \mu\text{m}$	$\approx 0.5 \mu\text{m}$	$2.5 \mu\text{m}$
Backsc. ratio	$\leq 1.2$	$\geq 1.2$	$\leq 2$	$\geq 2$	$\geq 2$
Depol. ratio	$\approx 1.5\%$	$\approx 1.5\%$	$> 5\%$	$\leq 5\%$	10 to 50%

which depolarize too weakly (depolarization  $\leq 5\%$ ) to be considered unequivocally as fully formed NAT particles, are included into the type Ib subclass.

We chose to characterize PSC by their optical properties at the maximum of backscatter ratio. The main reason is that the best signal-to-noise ratio is obtained at the peak, minimizing the uncertainties on the data set. Also, the signature of a PSC layer is thus determined at a single altitude point. Some PSCs extended through a relatively wide altitude range exhibiting distinct layers. In that case, each layer was treated as a distinct cloud which was characterized at its peak. Consequently, several PSCs might be observed on the same profile at different altitude levels.

According to the aerosol loading, two periods were analysed separately and then compared: before the eruption of Mount Pinatubo, 1989-1991, when only background aerosols are present; and after the eruption, 1992-1993, when a significant amount of volcanic aerosols was present.

#### 4.1. First Period: 1989-1991

During this period (April 1989 to August 1991), three different types of scattering layers were detected on the lidar signals between 8 and 25 km: background aerosols, cirrus, and PSCs [*Stefanutti et al.*, 1991].

Lidar measurements at 532 nm are sensitive to particles with radii greater than 0.1-0.15  $\mu\text{m}$ . Background aerosols were regularly observed between the tropopause and about 25 km. The altitude of maximum scattering varied between 15 and 21 km, depending on the tropopause height, with an average altitude at  $19.0 \pm 0.5$  km, which is in agreement with balloon-borne observations [*Rosen et al.*, 1975]. Backscatter ratios for background aerosols were first calculated from profiles obtained out of the PSC period (July and August). It showed little seasonal variations with a mean maximum backscatter ratio of 1.11 and a standard deviation  $\sigma$  of 0.08. The inclusion of July and August profiles, which did not exhibit PSC layers, in the calculation of the background aerosol average backscatter ratio profile does not change these values significantly. As expected, no depolarization was associated with background particulate matter.

Cirrus clouds are the second type of particles encountered in the altitude range of interest. From our lidar measurements, the properties of these clouds are close to those of type II PSC with backscatter ratios greater or equal to 2 and depolarization ratios ranging from 10 to 40%. However, cirrus clouds are expected to be found below or around the tropopause region (and they were). These cirrus observations are not discussed here.

During the period 1989-1991, we considered that PSCs were identified when the lidar signal indicated a depolarization ratio greater than 2.5% ( $1.5\% + 1.0\%$  originating from the maximum relative uncertainty at  $2\sigma$ ) and/or a backscatter ratio greater than the average backscatter ratio of background aerosols  $1.27 (1.11 + 0.16 \text{ at } 2\sigma)$ . The choice of the threshold values within their possible ranges should have little impact on the results, because most of the PSC identifications correspond to signals out of the  $2\sigma$  envelope. Individual PSC backscatter ratios are defined as the total backscatter minus the aerosol contribution. The aerosol contribution is estimated from the background aerosol mean profile.

#### 4.2. Second Period: 1992-1993

After a period of inactivity of 635 years, Mount Pinatubo ( $15.14^\circ\text{N}$ ,  $120.35^\circ\text{E}$ ), in the Philippines, erupted in June 1991 in series of minor explosions leading to a cataclysmic eruption on June 14 and 15. Large quantities of gaseous sulphur dioxide ( $\text{SO}_2$ ) were injected into the stratosphere between 20 and 30 km. The total mass of  $\text{SO}_2$  injected was estimated to be between 12,000 and 20,000 kT [*Bluth et al.*, 1992; *McPeters et al.*, 1993; *Read et al.*, 1993]. The  $\text{SO}_2$  cloud, as observed by Total Ozone Mapping Spectrometer (TOMS), encircled the Earth around the tropics in 22 days [*Bluth et al.*, 1992]. The conversion of gaseous  $\text{SO}_2$  into liquid sulphuric acid ( $\text{H}_2\text{SO}_4$ ) was completed within a few months. The meridional dispersion was driven by two transport regimes in the stratosphere [*Trepte et al.*, 1993]. A lower-altitude transport regime was induced by the Asian Monsoon anticyclonic circulation. At upper altitudes, poleward transport was associated with transient planetary wave activity interacting with the Quasi Biennial Oscillation (QBO) easterlies. Accord-

**Table 3.** Volcanic Cloud Maximum Backscatter ratio ( $R_{max}$ ) with 2 Standard Deviation and Altitude of This Maximum as Measured Inside Vortex by the POLE Lidar in Dumont d'Urville Between June and September in 1992 and 1993

		June	July	August	September
1992	$R_{max} (\pm 2\sigma)$	3.41 ( $\pm 1.53$ )	3.07 ( $\pm 0.80$ )	3.53 ( $\pm 1.26$ )	2.65 ( $\pm 0.75$ )
	Alt. of $R_{max}$	16.23 km	14.28 km	15.61 km	14.16 km
1993	$R_{max} (\pm 2\sigma)$	2.78 ( $\pm 1.12$ )	2.63 ( $\pm 1.42$ )	2.43 ( $\pm 1.54$ )	2.22 ( $\pm 0.92$ )
	Alt. of $R_{max}$	13.26 km	11.44 km	11.85 km	11.82 km

ing to POLE data, the volcanic cloud reached Dumont d'Urville in September 1991 outside of the vortex. After October 1991, the polar vortex was rarely located over the station. Then the aerosol loading increased continuously until December 1991. Dispersion and vertical mixing of the volcanic particles appeared to be completed by the end of February 1992 [David, 1995; Godin *et al.*, 1996].

Volcanic aerosols from the Cerro Hudson (49.9°S, 73.0°W) eruption (August 14 and 15, 1991) in Chile were first observed over Dumont d'Urville on September 6, 1991, below 15 km. They were totally removed from the Antarctic stratosphere at the beginning of 1992. These particles thus do not interfere with the present analyses.

In 1992-1993, the presence of dense volcanic particle layers in the lower stratosphere, made the distinction between type Ib PSCs and volcanic aerosols more difficult. The previous methodology for type Ib PSC identification had thus to be revised. Since volcanic particles have a composition and physical state similar to that of background aerosols, they were not expected to depolarize the lidar signal. Their only signature was an enhancement of backscatter ratio with respect to background aerosols values. The temporal evolution of the altitude and amplitude of the volcanic cloud maximum backscatter ratio inside the polar vortex is given in Table 3.

To reliably identify the type Ib cloud signatures superimposed on the volcanic aerosols backscatter signal, a two-step threshold type algorithm based on the observed variance of the volcanic cloud was developed. As dynamical transport through the polar vortex edge is small during the winter [Schoeberl *et al.*, 1992], with air inside the vortex experiencing subsidence, measurements located outside and inside vortex were treated independently. As the volcanic cloud underwent spatial and temporal fluctuations, daily backscatter ratio profiles were monthly averaged between June and September 1992 and 1993. First, all the profiles (with and without PSCs) were taken into account in the calculation of monthly mean profiles. Then, if a daily profile exhibited in certain regions deviations from the monthly mean larger than  $2\sigma$ , we considered that PSC layers were de-

tected on that profile. As a test, a new monthly mean profile was calculated without including the profiles on which PSCs were identified. Then the procedure was repeated. The resulting few additional PSC detections were found to be very close to the  $2\sigma$  envelope and thus doubtful. We decided to discard them from the PSC analysis. Therefore this method may underestimate the number of type Ib PSCs. Figure 4 shows some type Ib PSC profiles extracted by this procedure compared to the monthly mean profiles. As for the 1989-1991 period, the aerosol contribution is estimated from the new monthly mean profiles and individual PSC backscatter ratios correspond to the total backscatter from which the aerosol contribution was removed. Note that no PSCs were detected outside the vortex.

## 5. Results

Data collected during the pre-Pinatubo (1989-1991) and post-Pinatubo (1992-1993) periods were analyzed separately. The two data sets are compared and common features as well as differences are discussed. Sixty PSCs (any type) were detected in 1989-1991, whereas 61 PSCs (any type) were observed in 1992-1993, all located inside or at the edge of the polar vortex. Only five type II PSCs (one in 1989-1991 and four in 1992-1993) were detected, for temperatures below  $T_{ice}$ . Indeed, the evolution of the temperature profiles from radiosondes showed that temperatures very rarely dropped below  $T_{ice}$  over Dumont d'Urville. A climatological study cannot be completed and no clear definite conclusions on the effect of  $H_2SO_4$  aerosols loading on type II clouds formation could be directly inferred from the very few number of type II observations. Therefore they were excluded from further analysis. Measurements statistics on type I PSCs are given in Table 4.

Compared to higher-latitude stations [Collins *et al.*, 1993; Rosen *et al.*, 1993], PSCs were present over Dumont d'Urville relatively late in the season, mainly in July and August, reflecting the fact that the station was mostly inside the vortex during this time period. Some clouds were also detected in June and September, especially in 1992 and 1993. They were associated with the vortex moving over the station, providing suitable temperatures for PSC formation in June and September.

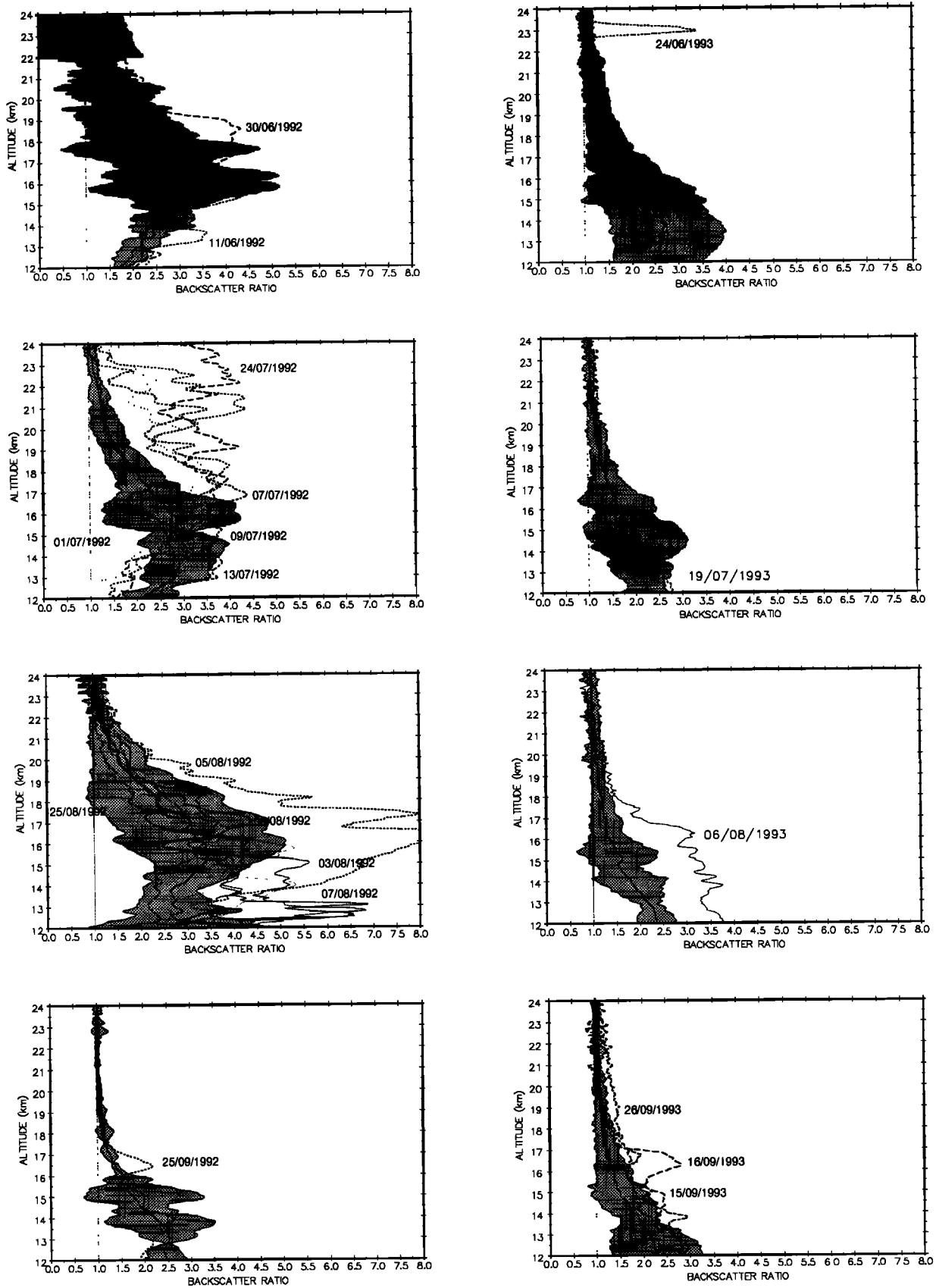


**Figure 4.** Type Ib PSC profiles extracted by the method using a threshold type algorithm based on the observed variance of the volcanic cloud compared to the monthly averaged profiles, for June to September 1992 and 1993. The grey envelope corresponds to the  $2\sigma$  standard deviation.

**Table 4.** Statistic of Type I PSC Observations

	1989-1991	1992-1993
Number of days of observations	31	25
Total number of observations	58	54
Number of observations with depolarization measurements*	47 (81.0%)	42 (77.8%)
Number of observations with radiosonde temperature measurements	32 (55.2%)	45 (83.5%)
Number of observations with both depolarization and radiosonde temperature measurements	29 (50.0%)	36 (66.7%)

\* Parentheses indicate percentage of the total number of PSC observations.

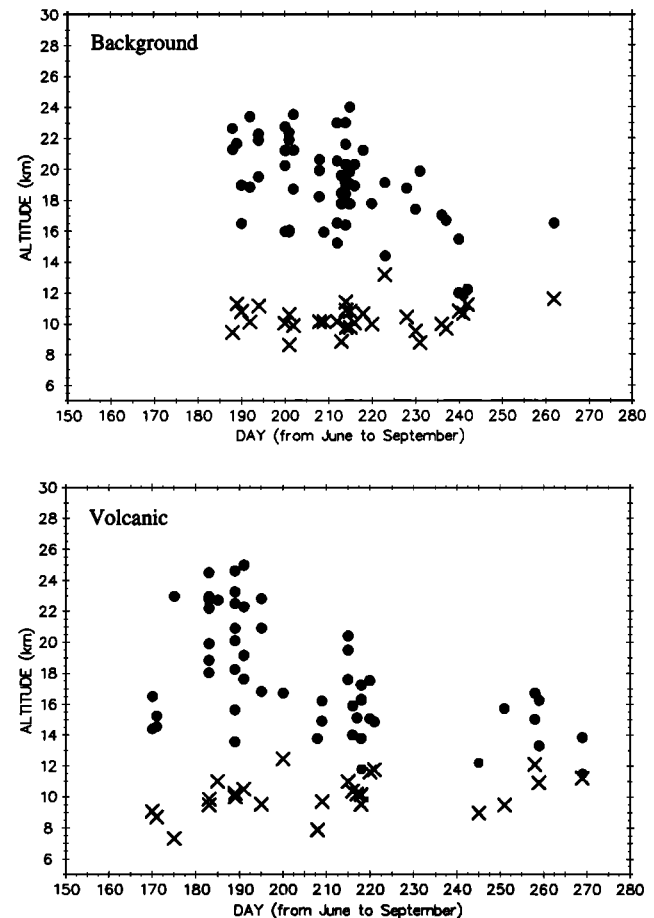
### 5.1. PSC Altitudes

Figure 5 shows the evolution of the altitude of the peak PSC scattering along with the tropopause height between June and September for both periods. PSCs were found between about 11 and 25 km. They were observed at higher altitudes at the beginning of the winter compared to the end, which is consistent with the stratospheric warming occurring first at higher altitudes [Iwasaka *et al.*, 1986]. Some clouds were detected at lower altitudes earlier in the winter in 1992-1993 than in 1989-1991. This appears more clearly on Figure 6, which displays the percentage of detected PSCs per 3-km-thick layers between 11 and 26 km. In 1989-1991, almost 70% of the PSCs were found between 17 and 23 km, around the peak in background sulphuric acid aerosols. In 1992-1993, the peak in PSC occurrence ( $\approx 73\%$  of the observations) was shifted toward lower altitudes, between 11 and 20 km, where most volcanic sulphuric acid aerosols were located. This tendency was also noticed over McMurdo station in 1992 [Deshler *et al.*, 1994].

### 5.2. PSC Temperatures

In order to account for the altitude dependency of the NAT point,  $T_{\text{NAT}}$ , the difference  $\Delta T_{\text{NAT}} (= T_{\text{NAT}} - T$ , where  $T$  is the radiosonde temperature) is used as an indicator of the potential for the formation of NAT PSCs.  $S_{\text{NAT}}$ , the saturation ratio of  $\text{HNO}_3$  with respect to NAT, is also a good indicator ( $S_{\text{NAT}} = P_{\text{HNO}_3} / P_{\text{HNO}_3}^s$ , where  $P_{\text{HNO}_3}$  is the nitric acid partial pressure and  $P_{\text{HNO}_3}^s$  the  $\text{HNO}_3$  equilibrium vapor pressure over NAT, for a given temperature and water vapor partial pressure). Both indicators,  $\Delta T_{\text{NAT}}$  or  $S_{\text{NAT}}$ , will be

used here interchangeably. The percentage of PSCs detected per 1 K class of  $\Delta T_{\text{NAT}}$  is shown on Figure 7. In 1989-1991, when PSCs were detected,  $\Delta T_{\text{NAT}}$  ranged from -2 to 6 K with a maximum occurrence between 1 and 4 K ( $\approx 73\%$  of the observations). Some clouds were observed at temperatures 2 K above the NAT point. However, this 2 K difference is not significant as it lies within the error of analysis resulting from the uncertainties in the radiosonde temperature and in the  $\text{HNO}_3$  mixing ratio (see section 3). Consequently, in view of this uncertainty, we do not claim to have detected PSCs above the reference NAT saturation temperature for background aerosols conditions. In 1992-1993,  $\Delta T_{\text{NAT}}$  ranged from -4 to 8 K. Despite two very cold cases during this period, more PSCs were observed at low temperature in 1989-1991 than in 1992-1993. This may only reflect interannual temperature variability. In contrast, PSC formation at higher temperatures is an interesting feature. Even allowing for a 2 K uncertainty, 18% of the PSC events for which radiosondes temperature measurements are available (see Figure 7), were found at temperatures above  $T_{\text{NAT}}$ .



**Figure 5.** Evolution of the altitude of the peak PSC scattering (dots) along with the tropopause height (crosses) between June and September, (top) for background conditions 1989-1991 and (bottom) for volcanic conditions 1992-1993.

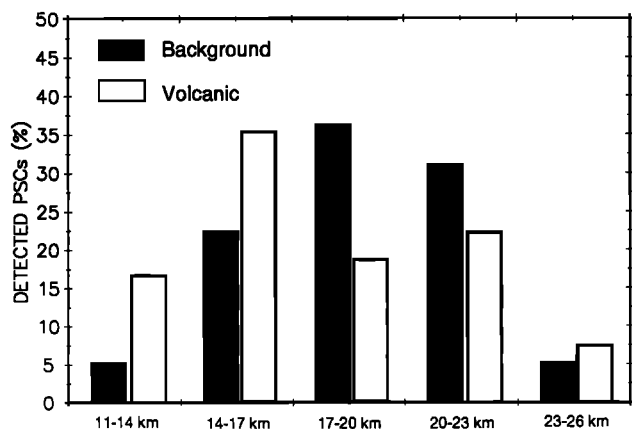


**Figure 6.** Percentage of PSCs detected per 3 km thick layer between 11 and 26 km, (top) for background conditions 1989-1991 and (bottom) for volcanic conditions 1992-1993.

In 1989-1991, the altitude of peak PSC scattering did not appear to be correlated with  $\Delta T_{NAT}$  (Figure 8). However, in 1992-1993, the PSCs observed at temperatures above  $T_{NAT}$  were all located below 17 km (i.e., 18% of the observed PSCs), around the center of the volcanic cloud.

### 5.3. PSC Types

As the different types of PSC were characterized through their backscatter ratio and depolarization ratio, the data should appear (for type I) as two distinct subclasses on a depolarization versus backscatter diagram. These diagrams are displayed in Figure 9; the solid lines are linear fits to the two subclasses, type Ia and Ib, for the pre-Pinatubo period. As explained in subsection 4.2, type Ia clouds are defined as clouds with a depolarization ratio greater than 5%. As expected, for both

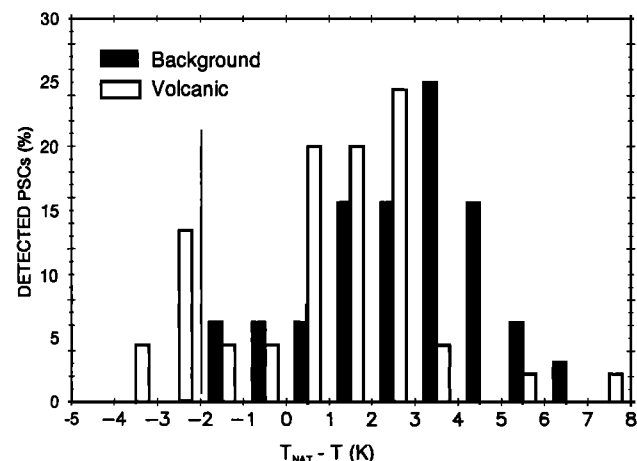


**Figure 7.** Percentage of PSCs detected per 1 K classes of  $\Delta T_{NAT}$  ( $= T_{NAT} - T$ , where  $T$  is the radiosonde temperature), (top) for background conditions 1989-1991 and (bottom) for volcanic conditions 1992-1993.

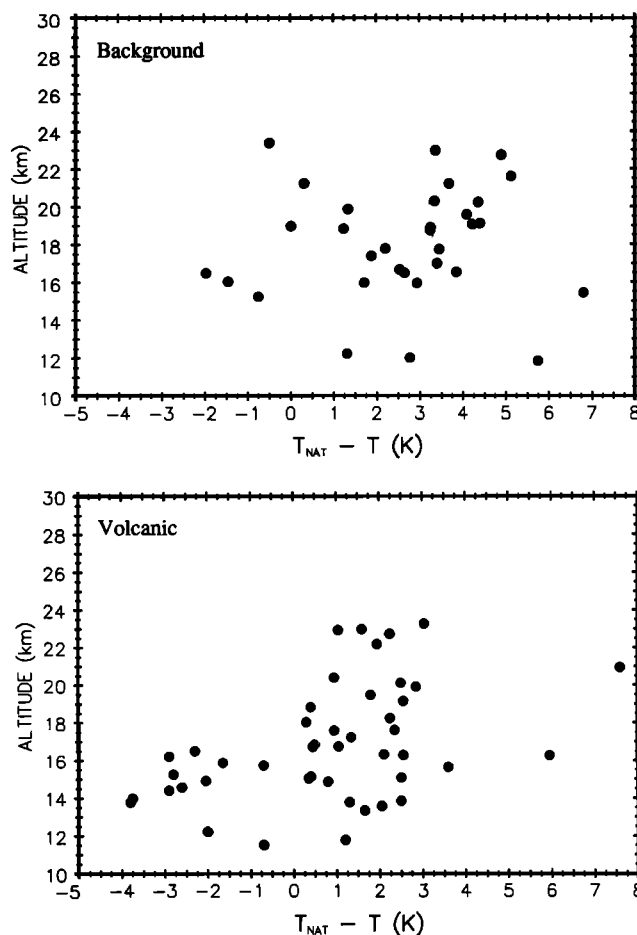


**Figure 8.** Altitude of peak PSC scattering as a function of  $\Delta T_{NAT}$ , (top) for background conditions 1989-1991 and (bottom) for volcanic conditions 1992-1993.

periods, type Ib data lay around a straight line corresponding to a constant low depolarization ratio and varying backscatter ratio. On the other hand, type Ia class exhibits high depolarization ratio and relatively low backscatter ratio (slope 0.16). The strong dispersion around the linear fit for type Ia may be due to the sampling of clouds at different stages of their formation and growth (that is, any stage: forming PSCs, mature clouds, or evaporating clouds).

Some differences are apparent between the two periods. Backscatter ratio of type Ia clouds ranges from 1 to 3 during the pre-Pinatubo period (1989-1991) whereas they essentially did not exceed  $\approx 2$  in post-Pinatubo conditions (1992-1993). In contrast, the range of backscatter ratio values covered by type Ib clouds was just slightly smaller during the pre-Pinatubo period (1 to 3.3) compared to the post-Pinatubo period (1 to 4.2, with two outliers at 6.1 and 7.6). As explained in subsection 4, PSC backscatter ratios were calculated as the difference between daily measured backscatter ratios and the aerosol contribution from monthly mean backscatter ratios. As expected, daily fluctuations were not significant for background conditions. On the other

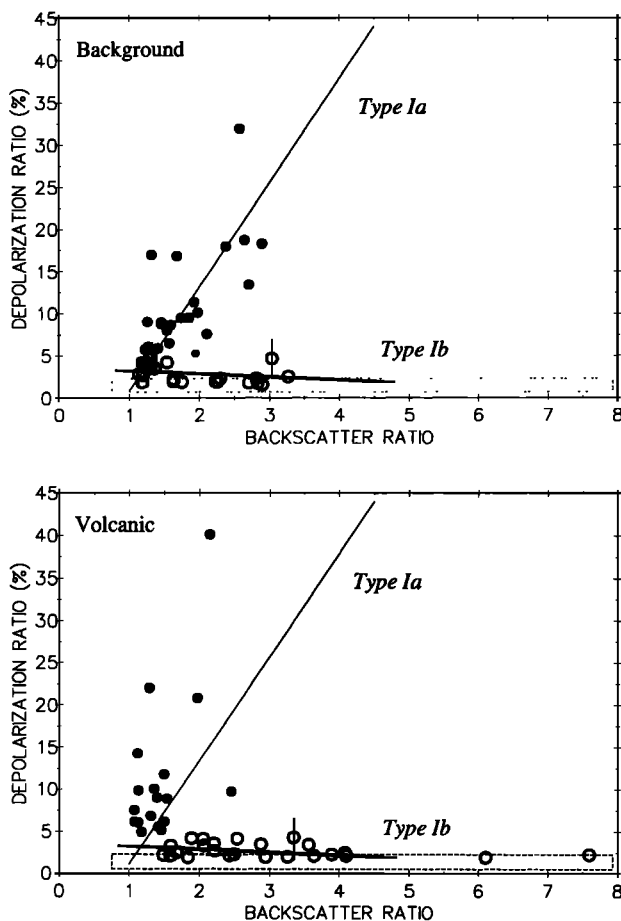


**Figure 9.** Depolarization ratio versus backscatter ratio diagram, where the two distinct subclasses of type I PSCs appear, (top) for background conditions 1989-1991 and (bottom) for volcanic conditions 1992-1993; linear fits to the two subclasses (solid lines), type Ia and Ib, for the 1989-1991 are reproduced on the 1992-1993 diagram; the rectangle indicates the range of depolarization uncertainty for type Ib ( $1.5\% + 0.5\%$  originating from the maximum relative uncertainty); an example of error bar is given for type Ib in each panel.

hand, they were very substantial for volcanic conditions. Thus the precision (sum of the daily signal standard deviation and the monthly mean standard deviation) on PSCs backscatter ratio values, for 1992-1993, was not sufficient for fully quantitative study of the effect of an enhanced aerosol loading on PSCs. For this reason, only the depolarization ratio is considered in the following analysis.

The percentage of PSCs detected per depolarization class is plotted in Figure 10. The frequency of depolarizing clouds (that is, depolarization ratio  $\geq 5\%$ ) represented 38% of the observations in post-Pinatubo conditions, which is 11% lower than during the pre-Pinatubo period. However, this difference is not statistically significant at the 95% confidence interval. Figure 11 shows the depolarization ratio as a function of  $\Delta T_{\text{NAT}}$ . Notice that only the PSC observations with measurements

of both depolarization and temperature are reported in figure 11. Only PSCs with non or low depolarization ratios were found at temperatures above  $T_{\text{NAT}}$ . In addition, it appears that as suggested by Figure 10, the fraction of type Ia out of the total PSCs observations was lower in 1992-1993 than in 1989-1991 although, on average, the levels of saturation with respect to NAT in both periods were comparable (see Figure 11). It is still possible that there were significant differences in temperatures and  $S_{\text{NAT}}$  between the two periods outside the Dumont D'Urville area, leading to changes in the distribution of PSCs over Dumont D'Urville.

## 6. Interpretation

### 6.1. Common Features

There are many common features in the pre-Pinatubo and post-Pinatubo climatologies. PSCs mainly occur when temperatures are low within or at the edge of the polar vortex. They tend to form around the altitude of the peak in sulphuric acid aerosol mixing ratio. This observed correlation implies that stratospheric aerosols may play a key role in PSC formation, probably acting as formation sites (condensation nuclei). Therefore, by changing the altitude of PSC formation, volcanic aerosols may have also influenced the altitude range of ozone destruction due to PSC heterogeneous chemistry.

It is very likely that the non depolarizing (type Ib) clouds are liquid, supporting strongly the existence of PSCs composed of liquid ternary  $\text{H}_2\text{SO}_4/\text{HNO}_3/\text{H}_2\text{O}$  solution [Molina *et al.*, 1993; Tabazadeh *et al.*, 1994]. Backscatter ratios can rapidly reach high values ( $R \geq 2$ ) as the entire population of small liquid particles grow by absorbing  $\text{HNO}_3$  available in the gas phase [Tabazadeh *et al.*, 1994]. This leads to high particles concentrations. The two outliers in backscatter ratio (6.1 and 7.6) for type Ib PSCs in 1992-1993 may reflect a higher number of particles (due to the enhanced

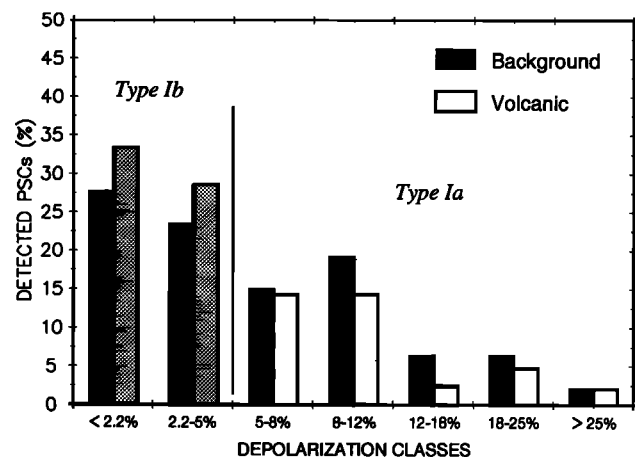


**Figure 10.** Percentage of PSCs detected per depolarization classes, (top) for background conditions 1989-1991 and (bottom) for volcanic conditions 1992-1993.

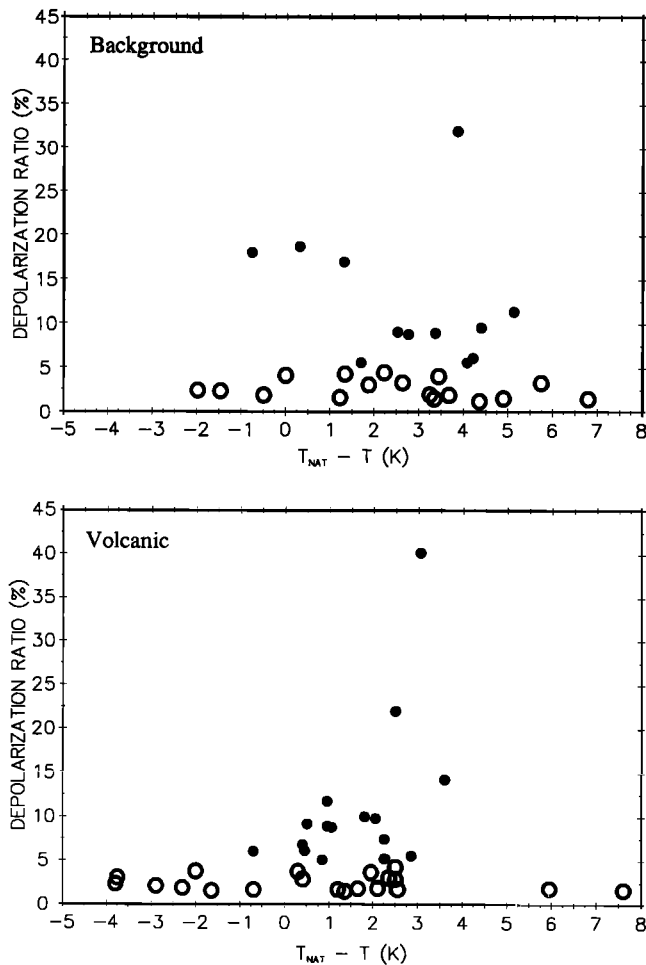


**Figure 11.** Depolarization ratio as a function of  $\Delta T_{\text{NAT}}$ , (top) for background conditions 1989-1991 and (bottom) for volcanic conditions 1992-1993; note that there are less depolarization data than backscatter data (see Figure 7).

number of formation sites) or higher sizes reached by type Ib particles (due to some temperature variability). Type Ib PSC were indeed found over a large range of temperature, even close to the frost point, demonstrating that they can stay liquid well below the NAT point. The dilution of  $\text{HNO}_3$  into the liquid droplets may explain why they do not crystallize readily [Carlsaw *et al.*, 1994]. Our observations of liquid PSCs well below the NAT point show that supersaturation with respect to NAT does not necessarily lead to the rapid formation of type Ia PSCs.

Depolarizing type Ia PSCs exhibit different values of backscatter ratios and depolarization ratios (this is the range expected for type Ia, both for backscatter ratio and depolarization ratio, see also Browell *et al.* [1990]). This variability may be indicative of observations at different growth stages and number densities or of the simultaneous presence of crystalline and residual liquid phases. MacKenzie *et al.* [1995] found that the  $\text{HNO}_3$  saturation ratio over NAT is greater than over

supercooled ternary solution and that, consequently, the growth rate of NAT particles is greater than the growth rate of ternary solution droplets for similar environmental conditions. Thus, once formed, NAT particles should grow through  $\text{HNO}_3$  uptake at the expense of the nucleation of additional NAT particles on ternary solution droplets. This could explain why the backscatter ratios we measured for type Ia PSCs remained low compared to type Ib PSCs. Solid-state particles were detected only at temperatures around and below the NAT point, indicating that NAT is, at least, heavily involved in their composition. The fact that type Ia PSCs were detected very close to  $T_{\text{NAT}}$  is not in conflict with the theory of type I PSC formation put forward by Tabazadeh *et al.* [1994]. They used Arctic measurements [Dye *et al.*, 1992; Kawa *et al.*, 1992] to show that type Ia clouds formed for  $S_{\text{NAT}}$  greater than 10, that is, when  $T$  is about 2-3 K below the NAT point. Laboratory experiments also suggest that NAT particles freeze out from ternary solution only for high saturation ratios [Molina *et al.*, 1993; Beyer *et al.*, 1994; Iraci *et al.*, 1995]. Koop *et al.* [1995] even indicate that aerosols droplets must first cool below the frost point and freeze out water ice before any sulphuric or nitric acid hydrates may form. In our case, PSCs could have been generated in the colder parts of the vortex, at high  $S_{\text{NAT}}$  or even below the frost point. Then, they could have been advected over Dumont d'Urville, as long as the ambient temperature remained below  $T_{\text{NAT}}$ . It is also possible that some of the type Ia PSCs were formed as soon as the NAT point was reached depending on the particular thermal history of the air masses [Tabazadeh *et al.*, 1996; David *et al.*, 1997]. However, this issue of a temperature hysteresis in the formation/evaporation cycle of type Ia PSCs cannot be addressed on the basis of our data only. Additional information such as the temperature history along the trajectories of the air masses is required.

No clearly depolarizing particles were detected above  $T_{\text{NAT}}$ . If some of the solid particles found around  $T_{\text{NAT}}$  were composed of SAT, they should have been observed at temperatures up to the SAT melting point (about 210-212 K at 50 hPa for typical stratospheric water vapor content [Beyer *et al.*, 1994]), largely above the NAT point ( $\approx 195$  K). According to Beyer *et al.* [1994],  $\text{H}_2\text{SO}_4/\text{H}_2\text{O}$  solutions are unlikely to freeze in the stratosphere. In contrast, Iraci *et al.* [1995] indicated that  $\text{H}_2\text{SO}_4$  often crystallizes to SAT, in agreement with microphysical calculations from MacKenzie *et al.* [1995]. Iraci *et al.* [1995] also pointed out that rapid crystallization of sulphuric acid at the onset of NAT growth is never observed: SAT do not accompany NAT formation. As sulphuric acid aerosols may remain highly supercooled, SAT could be found if temperatures have been within less than 5 K of the ice frost point for several days [Larsen *et al.*, 1995]. Accordingly, SAT could form in air parcels where NAT has not crystallized and which nevertheless have encountered low tempera-

tures. At the edge of the vortex, these two conditions may occur together only very rarely.

## 6.2. Differences Between the Two Climatologies

There are two main differences between the two PSCs climatologies. First, some type Ib PSCs were observed at temperatures a few degrees higher than  $T_{\text{NAT}}$  in 1992-1993. Second, the fraction of type Ia out of the total PSCs observed was lower in 1992-1993 than in 1989-1991 (see histogram of Figure 10). Although the difference was not highly statistically significant, it is worth testing if this apparent tendency is consistent with our theories on PSC formation.

The abundance of  $\text{HNO}_3$  may have been significantly different between 1989-1991 and 1992-1993. In volcanic conditions, as the surface area density of sulphuric acid particles are enhanced by up to a factor 100 [World Meteorological Organization, 1995], heterogeneous reactions on them led to an increase in  $\text{HNO}_3$  mixing ratios reaching values of 1 to 3 ppbv between 15 and 25 km during the 1992 winter and slightly less during the 1993 winter [Tie et al., 1994]. However, as most of the  $\text{NO}_y$  is already under the form of  $\text{HNO}_3$  at high latitudes in winter, the percentage changes in  $\text{HNO}_3$  concentrations would not have exceeded 20%. As shown previously, for such a small change in  $\text{HNO}_3$ , the increase in  $T_{\text{NAT}}$  would have been less than a few tenths of Kelvin, and the  $\text{HNO}_3$  saturation with respect to NAT should not occur at higher temperatures. Therefore the modest effect of enhanced aerosol loading on the abundance of gaseous  $\text{HNO}_3$  cannot account for a shift in type Ia occurrence.

A thermodynamical model of liquid ternary solution  $\text{H}_2\text{SO}_4/\text{HNO}_3/\text{H}_2\text{O}$  is used to investigate how a change in aerosol loading may have caused a shift in PSCs formation. This model is based on Carslaw et al. [1994, 1995] and calculates the particles composition as a function of temperature, pressure and total (gaseous + condensed)  $\text{H}_2\text{O}$ ,  $\text{HNO}_3$ , and  $\text{H}_2\text{SO}_4$  mixing ratio. Note that freezing processes are not modeled here.

The particle volume and the gas phase fraction of  $\text{HNO}_3$  following uptake by liquid  $\text{H}_2\text{SO}_4$  aerosols are plotted as a function of temperature in Figure 12 for three different sulphuric acid aerosol loadings (background, background  $\times 10$ , background  $\times 100$ , which is approximately the Pinatubo aerosol loading). For the background loading, as temperature decreases, the particle volume increases sharply at about 191-192 K. In contrast, for higher  $\text{H}_2\text{SO}_4$  aerosol loading, the particle volume increases smoothly. The  $\text{HNO}_3$  uptake becomes significant when the temperature falls below 200 K for volcanic conditions, whereas it occurs only around 193 K for background conditions (see Figure 12b). The reason for this temperature shift is the higher  $\text{H}_2\text{SO}_4$  mass available for  $\text{HNO}_3$  dissolution during the volcanic period. The substantial mass of  $\text{HNO}_3$  condens-

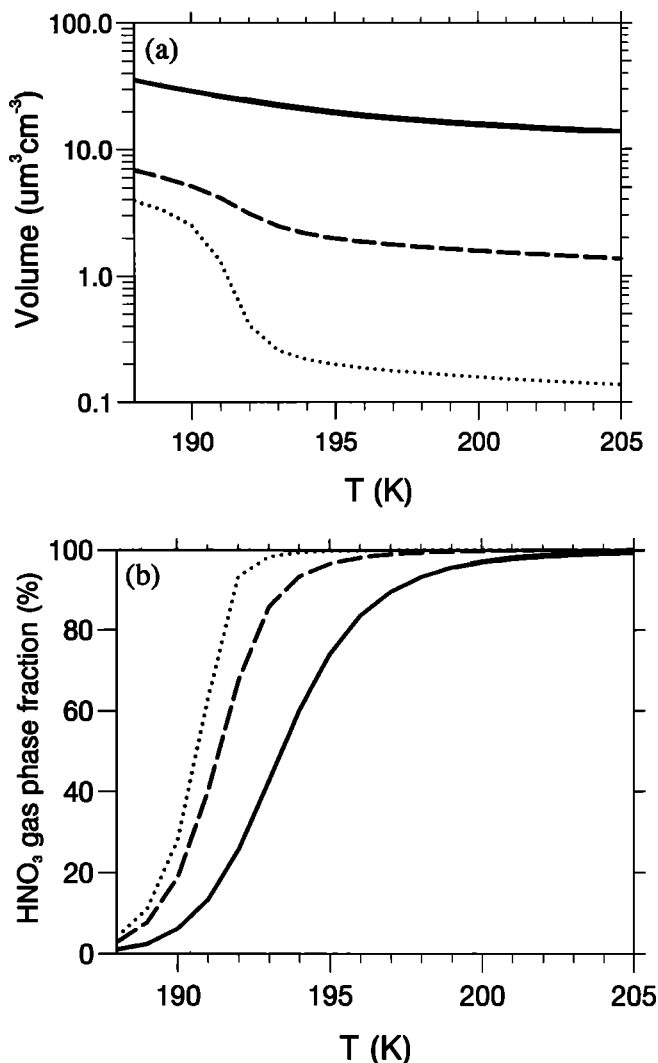


**Figure 12.** (top) Calculated particles volume and (bottom) gas phase fraction of  $\text{HNO}_3$  following uptake by liquid  $\text{H}_2\text{SO}_4$  aerosols as a function of temperature for three different sulphuric acid aerosol loadings: background ( $\text{H}_2\text{SO}_4 = 0.5$  ppbv, dotted line), background  $\times 10$  ( $\text{H}_2\text{SO}_4 = 5$  ppbv, dashed line), background  $\times 100$ , which is approximately the Pinatubo aerosol loading ( $\text{H}_2\text{SO}_4 = 50$  ppbv, solid line).

ing above  $T_{\text{NAT}}$  for volcanic aerosol contents could be at the origin of the high backscatter ratios, indicative of type Ib PSCs, observed above the NAT saturation point in 1992-1993. A theoretical study of the sensitivity of lidar backscatter response to changes in aerosol size distribution following  $\text{HNO}_3$  uptake is thus definitely warranted but is beyond the scope of the present work.

The effect of  $\text{HNO}_3$  uptake on  $S_{\text{NAT}}$  ( $\text{HNO}_3$  saturation over NAT greater than unity necessarily means temperature below  $T_{\text{NAT}}$ ) is illustrated in Figure 13. At low temperatures, as the aerosol loading increases,  $S_{\text{NAT}}$  decreases. This effect becomes significant below  $T_{\text{NAT}}$ . For example, the saturation ratio decreases

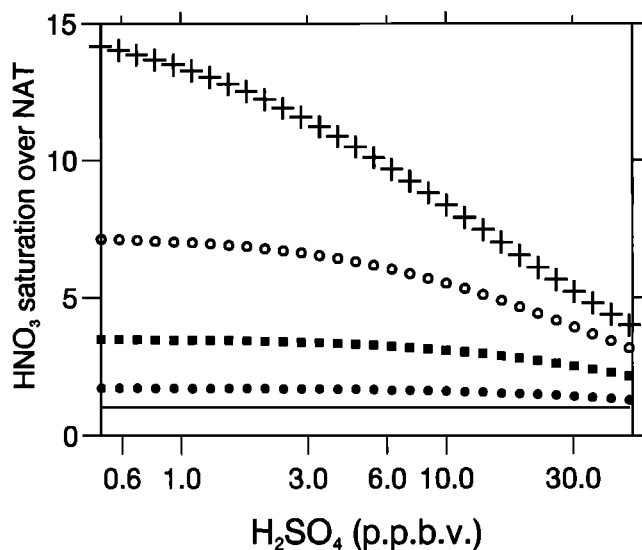


**Figure 13.** Calculated saturation ratio of  $\text{HNO}_3$  with respect to NAT as a function of  $\text{H}_2\text{SO}_4$  (ppbv) at 192 K (crosses), 193 K (circles), 194 K (squares), and 195 K (dots).

from 7 to 3 at 193 K while it drops from 14 to 4 at 192 K as the  $\text{H}_2\text{SO}_4$  mixing ratio increases. Theoretical [Tabazadeh *et al.*, 1994] and laboratory studies [Molna *et al.*, 1993; Beyer *et al.*, 1994; Iraci *et al.*, 1995] suggested that type Ia PSCs cannot form once  $T_{\text{NAT}}$  is reached, but rather that high  $\text{HNO}_3$  saturation ratios with respect to NAT are required to overcome a nucleation barrier. According to this formation mode and to our model calculations, highly enhanced aerosol loadings should be accompanied by a reduction in  $S_{\text{NAT}}$  for temperatures a few Kelvin below the NAT point, as compared to background loadings, resulting in a reduced probability of formation for type Ia PSCs. This mechanism was first pointed out by Carslaw *et al.* [1994]. Also, if type Ib PSCs act somehow as condensation nuclei for type Ia PSCs, a reduced formation of type Ia PSCs would favour the existence of type Ib clouds. Both effects are consistent with the shift in the respective fractions of type Ia and type Ib clouds observed from 1989-1991 to 1992-1993.

## 7. Summary and Conclusions

Lidar measurements of stratospheric aerosols and PSCs were routinely performed in Dumont d'Urville, Antarctica, between 1989 and 1993 within the framework of the NDSC. These long-term observations provide the first PSC climatology ever developed from lidar measurements, in Arctica or in Antarctica. It thus provides a database for a statistical analysis of type I PSC formation. Two different PSCs climatologies were produced according to the stratospheric sulphuric acid aerosol content, background aerosols in 1989-1991 and volcanic particles in 1992-1993, following the Mount

Pinatubo eruption. Comparisons of the pre-Pinatubo and post-Pinatubo climatologies allowed us to investigate the influence of the aerosol loading on PSCs formation. Very few type II clouds were detected; therefore only type I PSC observations are discussed here.

PSCs were mainly observed in July and August inside or at the edge of the polar vortex. Most of the PSCs tended to form around the peak in sulphuric acid aerosols, between 17 and 23 km in 1989-1991 (background conditions) and between 11 and 20 km in 1992-1993 (volcanic conditions). This tendency, which was also noticed over McMurdo station in 1992 [Deshler *et al.*, 1994], shows that sulphuric acid aerosols are very likely to act as condensation nuclei for PSCs. The formation of PSCs at lower altitude in 1992-1993, brought about by the presence of volcanic aerosols, may have had some implications for ozone losses at midlatitudes. Usually, PSCs form at an altitude range where there is little mixing and exchange of air masses between mid-latitude and polar regions (between 17 and 23 km in 1989-1991). However, mixing is much faster at the bottom part of the lower stratosphere. Therefore polar air, which had been chemically processed by PSCs, could have reached the midlatitudes more rapidly in 1992-1993. This may have been one of the mechanisms for the large ozone losses observed at southern midlatitudes in 1992 and 1993 [Gleason *et al.*, 1993].

As shown by previous lidar studies, two type I subclasses were identified: types Ia and Ib. A threshold temperature corresponding to the NAT saturation temperature is clearly noticeable for solid state particles (type Ia) during both periods. Allowing for a 2.5 K uncertainty in the estimation of NAT saturation temperature ( $T_{\text{NAT}}$ ) resulting from the uncertainties in the radiosonde temperature and in the  $\text{HNO}_3$  mixing ratio, no type Ia PSCs were detected above  $T_{\text{NAT}}$  in either climatology, lending support to the theory that NAT is the main component of type Ia PSCs. There was no evidence of the existence of SAT in the data.

Type Ib PSCs were even found throughout a large temperature range, even close to the frost point, showing that they can stay liquid well below the NAT point and that supersaturation with respect to NAT is a necessary, but not sufficient, condition for the existence of type Ia PSCs. Backscatter ratios for type Ib were found to cover a larger range of values (1.5 to 7.6) in 1992-1993 compared to 1989-1991 (1 to 3.3). In addition, in view of the uncertainties on radiosondes temperatures and  $\text{HNO}_3$  concentrations, no type Ib PSCs were unequivocally detected above  $T_{\text{NAT}}$  in 1989-1991, whereas it seems that  $\approx 18\%$  of the PSCs were found at temperatures above  $T_{\text{NAT}}$  in 1992-1993. This difference may be linked to the fact that the  $\text{HNO}_3$  uptake by volcanic sulphuric acid particles starts at higher temperatures, possibly above  $T_{\text{NAT}}$ . Alternatively, these PSCs above  $T_{\text{NAT}}$  might have been evaporating NAT particles because most of them were slightly depolarizing.

The fraction of type Ia out of the total PSCs observations was lower in 1992-1993 than in 1989-1991 although, on average, the levels of saturation with respect to NAT for both periods were comparable; however, this difference was not found to be highly statistically significant. Model calculations using a thermodynamic model of liquid ternary  $\text{H}_2\text{SO}_4/\text{HNO}_3/\text{H}_2\text{O}$  solution showed that, the high uptake of  $\text{HNO}_3$  by volcanic sulphuric acid aerosols around and below  $T_{\text{NAT}}$  could substantially reduce the level of saturation with respect to NAT. This may thus reduce the probability of formation of type Ia PSCs.

The interpretation of the PSC data of Dumont d'Urville presented here is mainly based on local measurements of temperature and on an equilibrium model of PSCs. This simple approach has some limitations. It does not allow us to investigate some aspects of the dynamics of the formation and evolution of PSCs. For example, additional information such as the temperature history along the trajectories of the PSCs air masses is required for addressing the issues of the temperature hysteresis in the formation/evaporation cycle of type Ia PSCs [Larsen *et al.*, 1995]. A more thorough analysis of the data is in progress using a three-dimensional Chemical Transport Model.

**Acknowledgments.** The logistics and the operations of the lidar are supported and funded by the Institut Français pour la Recherche et la Technologie Polaires (IFRTP). The authors wish to thank all members of the different teams of the IFRTP for their help in making this experiment a success, year after year. The authors also want to acknowledge L. Stefanutti, M. Morandi, M. Del-Guasta, and the whole Italian group involved in POLE. We thank R. Vautard and S. Edouard from Laboratoire de Météorologie Dynamique (CNRS) for providing potential vorticity maps, calculated from ECMWF analysis. We are grateful to K. Carslaw for providing parts of the thermodynamical model and to A.R. MacKenzie and J.A. Pyle for their help in setting up visits of C. David to the University of Cambridge. We also thank the two anonymous reviewers for their helpful comments on the manuscript.

## References

- Adriani, A., T. Deshler, G.P. Gobbi, B.J. Johnson, and G. Di Donfrancesco, Polar stratospheric clouds over McMurdo, Antarctica during the 1991 spring: Lidar and particle counter measurements, *Geophys. Res. Lett.*, **19**, 1755-1758, 1992.
- Beyer, K.D., S.W. Seago, H.Y. Chang, and M.J. Molina, Composition and freezing of aqueous  $\text{H}_2\text{SO}_4/\text{HNO}_3$  solutions under polar stratospheric conditions, *Geophys. Res. Lett.*, **21**, 871-874, 1994.
- Bluth, G.J.S., S.D. Doiron, C.C. Shnetzler, A.J. Krueger, and L.S. Walter, Global tracking of the  $\text{SO}_2$  clouds from the June 1991 Mount Pinatubo eruptions, *Geophys. Res. Lett.*, **19**, 151-154, 1992.
- Browell, E.V., C.F. Butler, S. Ismail, P.A. Robinette, A.F. Carter, N.S. Higdon, O.B. Toon, M.R. Schoeberl, and A.F. Tuck, Airborne lidar observations in the wintertime Arctic stratosphere: Polar stratospheric clouds, *Geophys. Res. Lett.*, **17**, 385-388, 1990.
- Carslaw, K.S., B.P. Luo, S.L. Clegg, T. Peter, P. Brimblecombe, and P.J. Crutzen, Stratospheric aerosol growth and  $\text{HNO}_3$  gas phase depletion from coupled  $\text{HNO}_3$  and water uptake by liquid particles, *Geophys. Res. Lett.*, **21**, 2479-2482, 1994.
- Carslaw, K.S., B. Luo, and T. Peter, An analytic expression for the composition of aqueous  $\text{HNO}_3\text{-H}_2\text{SO}_4$  stratospheric aerosols including gas phase removal of  $\text{HNO}_3$ , *Geophys. Res. Lett.*, **22**, 1877-1880, 1995.
- Chazette, P., C. David, J. Lefrère, S. Godin, and G. Mégie, Comparative lidar study of the optical, geometrical and dynamical properties of stratospheric post-volcanic aerosols, following the eruptions of El Chichon and Mount Pinatubo, *J. Geophys. Res.*, **100**, 23,195-23,207, 1995.
- Collins, R.L., K.P. Bowman, and C.S. Gardner, Polar Stratospheric Clouds at the South Pole in 1990: Lidar observations and analysis, *J. Geophys. Res.*, **98**, 1001-1010, 1993.
- Crutzen, P.J., and F. Arnold, Nitric acid cloud formation in the cold Antarctic stratosphere: a major cause for springtime ozone hole, *Nature*, **324**, 651-655, 1986.
- David, C., Etude des Nuages Stratosphériques Polaires et des aérosols volcaniques en régions polaires par sondage laser, Ph.D thesis, 273 pp., Univ. Paris VI Pierre et Marie Curie, Jan. 1995.
- David, C., S. Godin, G. Mégie, Y. Emery, and C. Flesia, Physical state and formation of Polar Stratospheric Clouds as inferred by the airborne lidar LEANDRE during SESAME, *J. Atmos. Chem.*, **27**, 1-16, 1997.
- Deshler, T., B.J. Johnson, and W.R. Rozier, Changes in the character of Polar Stratospheric Clouds over Antarctica in 1992 due to the Pinatubo volcanic aerosol, *Geophys. Res. Lett.*, **21**, 273-276, 1994.
- Dye, J.E., D. Baumgardner, B.W. Gandrud, S.R. Kawa, K.K. Kelly, M. Loewenstein, G.V. Ferry, K.R. Chan, and B.L. Gary, Particle size distributions in Arctic polar stratospheric clouds, growth and freezing of sulfuric acid droplets, and implications for cloud formation, *J. Geophys. Res.*, **97**, 8015-8034, 1992.
- Fiocco, G., M. Cacciani, P. di Girolamo, and D. Fua, Stratospheric cloud at South Pole during 1988, 1, Results of lidar observations and their relationship to temperature, *J. Geophys. Res.*, **97**, 5932-5946, 1992.
- Fox, L.E., D.R. Worsnop, M.S. Zahniser, and S.C. Wofsy, Metastable phases in polar stratospheric aerosols, *Science*, **267**, 351-355, 1995.
- Gille, J.C., J.M. Russell III, P.L. Bailey, E.E. Remsberg, L.L. Gordley, W.F.J. Evans, H. Fischer, B.W. Gandrud, A. Girard, J.E. Harries, and S.A. Beck, Accuracy and precision of the nitric acid concentrations determined by the Limb Infrared Monitor of the Stratosphere Experiment on NIMBUS 7, *J. Geophys. Res.*, **89**, 5179-5190, 1984.
- Gleason, J. F., et al., Record low global ozone, *Science*, **260**, 523-526, 1993.
- Gobbi, G.P., T. Deshler, A. Adriani, and D.J. Hofmann, Evidence for denitrification in the 1990 Antarctic spring stratosphere, I, Lidar and temperature measurements, *Geophys. Res. Lett.*, **18**, 1995-1998, 1991.
- Godin, S., C. David, and M. Guirlet, Evolution of the Mount Pinatubo volcanic cloud and analysis of its effect on the ozone amount as observed from ground-based measurements performed in Northern and Southern latitudes, edited by G. Fiocco, *NATO ASI Ser.*, **42**, 143-159, 1996.
- Hamill, P., R.P. Turco, and O.B. Toon, On the growth of nitric and sulfuric acid aerosol particles under stratospheric conditions, *J. Atmos. Chem.*, **7**, 287-315, 1988.
- Hanson, D.R., The vapor pressures of supercooled  $\text{HNO}_3/\text{H}_2\text{O}$  solutions, *Geophys. Res. Lett.*, **17**, 421-424, 1990.

- Hanson, D.R., and K. Mauersberger, Laboratory studies of the nitric acid trihydrate: Implications for the south polar stratosphere, *Geophys. Res. Lett.*, *15*, 855-858, 1988.
- Hofmann, D.J., and T. Deshler, Stratospheric cloud observations during formation of the Antarctic ozone hole in 1989, *J. Geophys. Res.*, *96*, 2897-2912, 1991.
- Iraci, L.T., A.M. Middlebrook, and M.A. Tolbert, Laboratory studies of the formation of polar stratospheric clouds: Nitric acid condensation on thin sulfuric acid films, *J. Geophys. Res.*, *100*, 20,969-20,977, 1995.
- Iwasaka, Y., T. Ono, and A. Nomura, Changes in the aerosol content and temperature in the Antarctic spring stratosphere: Lidar measurement at Syowa station (69°00'S, 39°35'E) in 1983, 1984 and 1985, *Geophys. Res. Lett.*, *13*, 1407-1410, 1986.
- Kawa, S.R., D.W. Fahey, K.K. Kelly, J.E. Dye, D. Baumgardner, B.W. Gandrud, M. Loewenstein, G.V. Ferry, and K.R. Chan, The Arctic polar stratospheric cloud aerosol: Aircraft measurements of reactive nitrogen total water and particles, *J. Geophys. Res.*, *97*, 7925-7938, 1992.
- Kent, G.S., L.R. Poole, and M.P. McCormick, Characteristics of Arctic polar stratospheric clouds as measured by lidar, *J. Atmos. Sci.*, *43*, 2149-2161, 1986.
- Kent, G.S., Poole L.R., McCormick M.P., Schaffner S.K., Hunt W.H., and Osborn M.T., Optical backscatter characteristics of Arctic Polar Stratospheric Clouds, *Geophys. Res. Lett.*, *17*, 377-380, 1990.
- Klett, J.D., Stable analytical inversion solution for processing lidar returns, *Appl. Opt.*, *20*, 211-220, 1981.
- Klett, J.D., Lidar inversion with variable backscatter/extinction ratios, *Appl. Opt.*, *24*, 1638-1643, 1985.
- Koop, T., U.M. Biermann, W. Raber, B.P. Luo, P.J. Crutzen, and T. Peter, Do stratospheric aerosol droplets freeze above the ice frost point?, *Geophys. Res. Lett.*, *22*, 917-920, 1995.
- Larsen, N., J.M. Rosen, N.T. Kjome, and B. Knudsen, Deliquescence and freezing of stratospheric aerosols observed by balloonborne backscatter sondes, *Geophys. Res. Lett.*, *22*, 1233-1236, 1995.
- MacKenzie, A.R., M. Kulmala, A. Laaksonen, and T. Vesala, On the theories of type I polar stratospheric cloud formation, *J. Geophys. Res.*, *100*, 11,275-11,288, 1995.
- McCormick, M.P., H.M. Steele, P. Hamill, W.P. Chu, and T.J. Swisler, Polar stratospheric cloud sightings by SAM II, *J. Atmos. Sci.*, *39*, 1387-1397, 1982.
- McNeil, W.R., and A.I. Carswell, Lidar polarization studies of the troposphere, *Appl. Opt.*, *14*, 2158-2178, 1975.
- McPeters, R.D., The atmospheric SO<sub>2</sub> budget for Pinatubo derived from NOAA-11 SBUV/2 spectral data, *Geophys. Res. Lett.*, *20*, 1971-1974, 1993.
- Meilinger, S.K., T. Koop, B.P. Luo, T. Huthwelker, K.S. Carslaw, U. Krieger, P.J. Crutzen, and T. Peter, Size-dependent stratospheric droplet composition in lee wave temperature fluctuations and their potential role in PSC freezing, *Geophys. Res. Lett.*, *22*, 3031-3034, 1995.
- Molina, M.J., R. Zhang, P.J. Woolbridge, J.R. McMahon, J.E. Kim, H.Y. Chang, and K.D. Beyer, Physical chemistry of the H<sub>2</sub>SO<sub>4</sub>/HNO<sub>3</sub>/H<sub>2</sub>O system: Implications for polar stratospheric clouds, *Science*, *251*, 1418-1423, 1993.
- Murray, F.W., On the computation of saturation vapor pressure, *J. Appl. Meteorol.*, *6*, 203-204, 1967.
- Parsons, C.L., G.A. Norcross, and R.L. Brooks, Radiosonde pressure sensor performance: Evaluation using tracking radars, *J. Atmos. Oceanic Tech.*, *1*, 321-327, 1984.
- Platt, C.M.P., Remote sounding of high clouds, III - Monte Carlo calculation of multiple scattered lidar returns, *J. Atmos. Sci.*, *38*, 156-167, 1981.
- Poole, L.R., and M.P. McCormick, Polar stratospheric clouds and the Antarctic ozone hole, *J. Geophys. Res.*, *93*, 8423-8430, 1988.
- Read, W.G., L. Froidevaux, and J.W. Waters, Microwave Limb Sounder measurement of stratospheric SO<sub>2</sub> from the Mt. Pinatubo volcano, *Geophys. Res. Lett.*, *20*, 1299-1302, 1993.
- Roche, A.E., J.B. Kumer, J.L. Mergenthaler, R.W. Nightingale, W.G. Uplinger, G.A. Ely, J.F. Potter, D.J. Wuebbles, P.S. Connell, and D.E. Kinnison, Observations of lower-stratospheric CLONO<sub>2</sub>, HNO<sub>3</sub>, and aerosols by the UARS CLAES experiment between January 1992 and April 1993, *J. Atmos. Sci.*, *51*, 2877-2902, 1994.
- Rosen, J.M., D.J. Hofmann, and J. Laby, Stratospheric aerosols measurements, II, The world-wide distribution, *J. Atmos. Sci.*, *32*, 1457-1462, 1975.
- Rosen, J.M., and D.J. Hofmann, Optical modelling of stratospheric aerosols: Present status, *Appl. Opt.*, *25*, 23, 410-419, 1986.
- Rosen, J.M., W.T. Kjome, and S.J. Oltmans, Balloon borne observations of backscatter, frost point and ozone in polar stratospheric clouds at the South Pole, *Geophys. Res. Lett.*, *18*, 171-174, 1991.
- Rosen, J.M., W.T. Kjome, and S.J. Oltmans, Simultaneous ozone and polar stratospheric clouds observations at South Pole station during and spring 1991, *J. Geophys. Res.*, *98*, 12,741-12,751, 1993.
- Sacco, V.M., F. Castagnoli, M. Morandi, and L. Stefanutti, Elastic backscattering lidar system for atmospheric measurements in Antarctica, *Opt. Quantum Electron.*, *21*, 215, 1989.
- Schoeberl, M.R., L.R. Lait, P.A. Newman, and J.E. Rosenfield, The structure of the polar vortex, *J. Geophys. Res.*, *97*, 7859-7882, 1992.
- Stanford, J.L., Possible sink for stratospheric water vapor at the winter Antarctic pole, *J. Atmos. Sci.*, *30*, 1431-1436, 1973.
- Steele, H.M., and P. Hamill, Effects of temperature and humidity on the growth and optical properties of sulfuric acid-water droplets in the stratosphere, *J. Aerosol Sci.*, *12*, 517-528, 1981.
- Stefanutti, L., M. Morandi, M. DelGuasta, S. Godin, G. Mégie, J. Brechet, and J. Picquard, Polar stratospheric cloud observations over the Antarctic continent at Dumont d'Urville, *J. Geophys. Res.*, *96*, 12,975-12,987, 1991.
- Stefanutti, L., F. Castagnoli, M. Del Guasta, M. Morandi, V.M. Sacco, L. Zuccagnoli, S. Godin, G. Mégie, and J. Porteneuve, The Antarctic ozone lidar system, *Appl. Phys. B*, *55*, 3-12, 1992.
- Tabazadeh, A., R.P. Turco, K. Drdla, and M.Z. Jacobson, A study of type I polar stratospheric clouds formation, *Geophys. Res. Lett.*, *21*, 1619-1622, 1994.
- Tabazadeh, A., O.B. Toon, and P. Hamill, Freezing behavior of stratospheric sulfate aerosols inferred from trajectory studies, *Geophys. Res. Lett.*, *22*, 1725-1725, 1995.
- Tabazadeh, A., O.B. Toon, B.L. Gary, J.T. Bacmeister, and M.R. Schoeberl, Observational constraints on the formation of type Ia polar stratospheric clouds, *Geophys. Res. Lett.*, *23*, 2109-2112, 1996.
- Tie, X.X., G.P. Brasseur, B. Briegleb, and C. Granier, Two-dimensional simulation of Pinatubo aerosol and its effect on stratospheric ozone, *J. Geophys. Res.*, *99*, 20,545-20,562, 1994.
- Toon, O.B., P. Hamill, R.P. Turco, and J. Pinto, Condensation of HNO<sub>3</sub> and HCl in the winter polar stratosphere, *Geophys. Res. Lett.*, *13*, 1284-1287, 1986.
- Toon, O.B., R.P. Turco, J. Jordan, J. Goodman, and G.V. Ferry, Physical processes in polar stratospheric clouds, *J. Geophys. Res.*, *94*, 11,359-11,380, 1989.

- Toon, O.B., E.V. Browell, S. Kinne, and J. Jordan, An analysis of lidar observations of Polar Stratospheric Clouds, *Geophys. Res. Lett.*, *17*, 393-396, 1990.
- Trepte, C.R., R.E. Veiga, and M.P. McCormick, The poleward of dispersion of Mount Pinatubo Volcanic Aerosol, *J. Geophys. Res.*, *98*, 18,563-18,573, 1993.
- Tuck, A.F., R.T. Watson, E.P. Condon, J.J. Margitan, and O.B. Toon, The planning and execution of ER-2 and DC-8 aircraft flights over Antarctica, August and September 1987, *J. Geophys. Res.*, *94*, 11,181-11,222, 1989.
- Tuck, A.F., et al., Polar stratospheric cloud processed air and potential vorticity in the northern hemisphere lower stratosphere at mid-latitudes during winter, *J. Geophys. Res.*, *97*, 7883-7904, 1992.
- Worsnop, D.R., L.E. Fox, M.S. Zahniser, and S.C. Wofsy, Vapor pressures of solid hydrates of nitric acid: Implications for Polar Stratospheric Clouds, *Science*, *259*, 71-74, 1993.
- World Meteorological Organization, Scientific Assessment of Ozone Depletion: 1994, *WMO Global Ozone Research and Monitoring Project, Rep. 37*, Geneva, Switzerland, 1995.
- 
- Slimane Bekki, Christine David, Sophie Godin and Gérard Mégie, Service d'Aéronomie du CNRS, Institut Pierre-Simon Laplace, Université Paris VI, Boîte 102, 4 place Jussieu, 75252 Paris Cedex 05, France. (e-mail: Christine.David@aero.jussieu.fr)
- Martyn P. Chipperfield, Department of Chemistry, University of Cambridge, Lensfield Road, Cambridge CB2 1EW, U.K. (e-mail: martyn@atm.ch.cam.ac.uk)

(Received April 9, 1997; revised May 6, 1998; accepted May 14, 1998.)